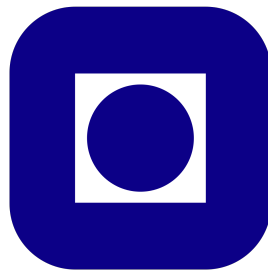


AREA

THEME

Title



Henrik Døvre Andrews
Norwegian university of Science and Technology

December 29, 2023

Abstract

Lorem ipsum dolor sit amet, consectetur adipiscing elit. Ut purus elit, vestibulum ut, placerat ac, adipiscing vitae, felis. Curabitur dictum gravida mauris. Nam arcu libero, nonummy eget, consectetur id, vulputate a, magna. Donec vehicula augue eu neque. Pellentesque habitant morbi tristique senectus et netus et malesuada fames ac turpis egestas. Mauris ut leo. Cras viverra metus rhoncus sem. Nulla et lectus vestibulum urna fringilla ultrices. Phasellus eu tellus sit amet tortor gravida placerat. Integer sapien est, iaculis in, pretium quis, viverra ac, nunc. Praesent eget sem vel leo ultrices bibendum. Aenean faucibus. Morbi dolor nulla, malesuada eu, pulvinar at, mollis ac, nulla. Curabitur auctor semper nulla. Donec varius orci eget risus. Duis nibh mi, congue eu, accumsan eleifend, sagittis quis, diam. Duis eget orci sit amet orci dignissim rutrum.

Summary

Nam dui ligula, fringilla a, euismod sodales, sollicitudin vel, wisi. Morbi auctor lorem non justo. Nam lacus libero, pretium at, lobortis vitae, ultricies et, tellus. Donec aliquet, tortor sed accumsan bibendum, erat ligula aliquet magna, vitae ornare odio metus a mi. Morbi ac orci et nisl hendrerit mollis. Suspendisse ut massa. Cras nec ante. Pellentesque a nulla. Cum sociis natoque penatibus et magnis dis parturient montes, nascetur ridiculus mus. Aliquam tincidunt urna. Nulla ullamcorper vestibulum turpis. Pellentesque cursus luctus mauris.

Acknowledgments

Nulla malesuada porttitor diam. Donec felis erat, congue non, volutpat at, tincidunt tristique, libero. Vivamus viverra fermentum felis. Donec nonummy pellentesque ante. Phasellus adipiscing semper elit. Proin fermentum massa ac quam. Sed diam turpis, molestie vitae, placerat a, molestie nec, leo. Maecenas lacinia. Nam ipsum ligula, eleifend at, accumsan nec, suscipit a, ipsum. Morbi blandit ligula feugiat magna. Nunc eleifend consequat lorem. Sed lacinia nulla vitae enim. Pellentesque tincidunt purus vel magna. Integer non enim. Praesent euismod nunc eu purus. Donec bibendum quam in tellus. Nullam cursus pulvinar lectus. Donec et mi. Nam vulputate metus eu enim. Vestibulum pellentesque felis eu massa.

Contents

1	Introduction	7
2	The ever-expanding Universe	8
2.1	Cosmological parameters	8
2.2	Shape of the Universe	8
2.3	Redshift	9
2.4	Comoving distance	9
2.5	Luminosity distance	10
3	High energy particles	11
3.1	Acceleration of high energy particles	11
3.2	UHECRs	12
3.2.1	Production and Energy loss	12
3.2.2	Detection	13
3.2.3	Emissivity estimates	13
3.3	Neutrinos	14
3.3.1	Production and Energy loss	14
3.3.2	Detection	15
3.3.3	Emissivity estimates	16
4	Active galactic nuclei	17
4.1	AGN structure and classification	17
4.1.1	Accretion disk	17
4.1.2	Corona and X-ray emission	19
4.1.3	Broad and narrow line region	19
4.1.4	Dust torus	19
4.1.5	Jets	19
4.2	Types of AGNs	20
5	Luminosity functions	21
5.1	X-ray LF	21

6	Evolution	25
6.1	Luminosity distribution	25
6.2	Density distribution	27
6.3	Expected luminosity	28
7	Energy budget estimation	31
7.1	UHECRs emissivity	31
7.2	Neutrino emissivity	32
8	Conclusion	35

List of Figures

1	Hillas criterion for proton (blue line) and iron (red line) accelerated up to $10^{20}eV$ and $10^{21}eV$ respectively. Image taken from Kotera and Olinto 2011	12
2	The diffuse flux of UHECRs as measured by the Pierre Auger Observatory and the Telescope Array. The flux is separated into galactic and extra galactic sources where the total spectrum follows the black dots. Image taken from Abdul Halim et al. 2023	13
3	The IceCube neutrino observatory. The detector is located at the South Pole and is a large block of ice instrumented with photomultiplier tubes. Image taken from Andeen and Plum 2019	15
4	The diffuse flux of neutrinos as measured by the Ice Cube observatory. The y-axis on the left image is the number of events per bin. The flux is separated into contributions from atmospheric neutrinos and astrophysical neutrinos. The right image is the model astrophysical flux as measured by ICE CUBE. Images taken from Abbasi et al. 2022	16
5	AGN unification	18
6	Luminosity density for the different classes of AGNs. The different classes are defined in the title as well as the chosen LF model.	26
7	Density distribution for the four different classes of AGNs. The different classes are defined in the title as well as the chosen LF model.	27
8	Expected luminosity and emissivity for the four different classes of AGNs. The different classes are defined in the title as well as the chosen LF model.	29
9	UHECR emissivity for the four different classes of AGNs.	31
10	Neutrino emissivity for the four different classes of AGNs.	32
11	Diffuse neutrino flux for the four different classes of AGNs.	33

List of Tables

1	The model parameters for the astrophysical flux of neutrinos as measured by the Ice Cube observatory.	16
2	X-ray LF parameters, a , normalized by a factor of 10^{-7} , b , normalized by a factor of 10^{44} c, has more factors that do not fit in the table, $z_{c2} = 3$, $\alpha_2 = -0.1$, $L_{c2} = 10^{44}$, $v_3 = -6.2$, $\beta = 0.84$	22
3	Luminosity range for different models	22

-abstract -sammendrag -acknowledgments -list of figure -list of tables

1 Introduction

2 The ever-expanding Universe

To investigate sources very far away from an observer it is important to understand the influence this distance has on the desired observables. Therefore, in astrophysics and astronomy in general there are distances created to take into account the effects of an expanding Universe. This chapter draws heavily from Hogg 2000.

2.1 Cosmological parameters

A reasonable place to start is with the Hubble constant H_0 . This parameter sets the recession speed of a point at proper distance d and the current position via this relation $v = H_0 d$. The subscript 0 refers to the present epoch signifying that H_0 is not static but changes with time. The precise value of H_0 is quite debated, so it's commonly expressed in a parameterised form,

$$H_0 = 100 \frac{\text{km}}{\text{s}} \frac{1}{\text{Mpc}} h.$$

The parameter h is a dimensionless number that according to current knowledge can take the value between 0.5 to 0.8 reflecting the range of answers collected from recent work.

Beyond its basic definition, H_0 also allows for the derivation of two significant cosmic scales:

Hubble Time (t_H) : Defined as the inverse of H_0 , t_H provides an estimate of the age of the Universe. It sets a scale for the time since the Big Bang, assuming the Universe has been expanding at a constant rate. The equation $t_H = 1/H_0 \approx 14$ Billion years offers a way to approximate this expansion timescale.

Hubble Distance (D_H) : This is a measure of the distance. Calculated as $D_H = c/H_0 \approx 4.4$ Gly, where c is the speed of light, it represents a critical boundary in observational cosmology.

2.2 Shape of the Universe

The shape and expansion of the Universe are central themes in cosmology, but first one needs to define the structure of the Universe and its contents. In this report and many articles, the Universe is often explored through the lens of the flat Lambda Cold Dark Matter (Λ CDM) model. This model, widely accepted in contemporary cosmology, provides a framework for understanding the Universe's composition and its expansion dynamics by assuming as the name suggests no curvature. In the Λ CDM model, two key parameters are important: the mass density of the Universe, ρ_0 , and the cosmological constant, Λ . These parameters, which evolve, are a part of defining the metric tensor in general relativity, thereby allowing us to model the curvature of the Universe based on its initial conditions. These parameters are often expressed as dimensionless variables:

$$\Omega_m = \frac{8\pi G \rho_0}{3H_0^2}$$

$$\Omega_\Lambda = \frac{\Lambda c^2}{3H_0^2}$$

Here, Ω_m represents the matter density parameter, encompassing both ordinary (baryonic) matter and dark matter. Ω_Λ , on the other hand, corresponds to the density parameter associated with the cosmological constant, which is often interpreted as dark energy.

In general, one has a third density parameter Ω_k which defines the curvature of space-time and the relationship between these parameters is expressed as:

$$\Omega_m + \Omega_\Lambda + \Omega_k = 1$$

In a flat Universe, one has $\Omega_k = 0$ and the Universe is dominated by dark energy and dark matter. The model used in this report and the papers used in the following chapters is the flat Λ CDM model where the parameters take the values of $\Omega_\Lambda = 0.7$ and $\Omega_m = 0.3$. These values align with current observational data.

2.3 Redshift

Redshift is defined as the fractional Doppler shift of emitting light. The Doppler effect is a known effect on different observables in the Universe where the relative motion of sources to observers will impact the observable. The redshift is quantified for a light source as

$$z = \frac{\nu_e}{\nu_o} - 1 = \frac{\lambda_o}{\lambda_e} - 1 \quad (1)$$

Here o refers to the observed quantity and e the emitted. Due to the expansion of the Universe the light emitted from a distant source will be increasingly redshifted the further away it is. In these scenarios the redshift serves as a distance measure, allowing us to deduce distances to faraway objects.

2.4 Comoving distance

Comoving distance is an important concept in cosmography, acting as a standard unit for various distance measurements in the Universe. This distance, often termed the line-of-sight distance for an observer on Earth, remains constant even as objects expand with the Hubble flow. To calculate the total comoving distance (D_c) to an object, one integrates the differential comoving distances (δD_c) along the line of sight, starting from redshift $z = 0$ to the object. This integration necessitates consideration of the Universe's parametric composition and the δD_c is expressed as

$$\delta D_c = \frac{D_H}{E(z)} dz, \quad (2)$$

where the function $E(z)$ is defined as

$$E(z) = \sqrt{\Omega_m(z+1)^3 + \Omega_k(1+z)^2 + \Omega_\Lambda}. \quad (3)$$

Here, $E(z)$ incorporates the density parameters previously discussed and the redshift z . It also relates to the Hubble constant observed by a hypothetical observer at redshift z , expressed as $H(z) = H_0 E(z)$.

One then calculates the comoving distance D_c from

$$D_c = D_H \int_0^z \frac{dz}{E(z)} \quad (4)$$

In addition to the line of sight, one needs to define the transverse comoving distance D_m . This distance relates two points in the night sky at the same redshift separated by an angle $d\theta$. The actual distance between them $d\theta D_m$ will then vary depending on the curvature of the Universe. This relationship is summarized in the following equation which accounts for different geometries,

$$D_m = \begin{cases} D_H \frac{1}{\sqrt{\Omega_k}} \sinh\left(\frac{\sqrt{\Omega_k} D_c}{D_H}\right) & \text{if } \Omega_k > 0 \\ D_c & \text{if } \Omega_k = 0 \\ D_H \frac{1}{\sqrt{|\Omega_k|}} \sin\left(\frac{\sqrt{|\Omega_k|} D_c}{D_H}\right) & \text{if } \Omega_k < 0 \end{cases}$$

The different cases correspond to hyperbolic, flat, and spherical geometry respectively. The true nature of the Universe is still unknown, but recent observations indicate a flat Universe.

2.5 Luminosity distance

The luminosity distance D_l is defined through the relation between the bolometric flux F of a source and its bolometric luminosity L . Bolometric flux is the energy received per unit of time per unit area without any obscuration, while bolometric luminosity is the total energy emitted per unit of time. The luminosity distance is defined as

$$D_l = \sqrt{\frac{L}{4\pi F}} \quad (5)$$

This formula reflects how the observed flux at the observer's location differs based on the distance from the source and the intrinsic luminosity emitted.

It is related to the transverse comoving distance via

$$D_l = (1 + z)D_m. \quad (6)$$

If one wants to calculate the spectral flux/ differential flux one needs to take into account a correction. This correction comes from the fact that one is viewing a redshifted object. The object is emitting in a different band than observed. The spectrum of the differential flux F_ν is related to the spectral luminosity via

$$F_\nu = (1 + z) \frac{L_{(1+z)\nu}}{L_\nu} \frac{L_\nu}{4\pi D_l^2}. \quad (7)$$

All these equations listed help include the effects of an expanding Universe when astronomers study distant objects and their properties.

3 High energy particles

In this chapter, I will discuss the different types of high-energy particles that are of interest in this paper, i.e. neutrinos and ultra-high energy cosmic rays (UHECRs). I will briefly discuss their generation and how they are detected. Then introduce how they lose energy in their journey to the Earth, and lastly calculate the emissivity of their hypothetical sources from the ground observations here on earth.

3.1 Acceleration of high energy particles

To reach high energy, particles need to be accelerated. Knowing the exact source of acceleration can be difficult since we do not know the sources, but one can put constraints on any source given some simple arguments. By arguing that the acceleration needs to be of a certain strength and that the particle being accelerated needs to stay confined within the accelerator for long enough one can put constraints on the source. This is called the Hillas criterion and is a way of estimating the maximum energy a particle can reach in a given source.

For relativistic particles with charge Z and energy ϵ in a magnetic field of strength B one can define the Larmor radius

$$R_L = \frac{\epsilon}{ZB} \quad (8)$$

By arguing that the definition of confinement of a particle to a source is by equating the Larmor radius to the size of the source one can easily derive the maximum achievable energy for a particle as follows.

$$\epsilon_{max} = ZBR \quad (9)$$

Via this method, one can illustrate the potential candidates needed to produce the required and importantly observed high-energy particles. This requirement is named the Hillas criterion after G. Hillas who first proposed this method Hillas 1984. The criterion works as an upper boundary of acceleration sources since it does not account for energy loss in the acceleration process or any type of interaction that one could expect to be in turbulent environments. In figure 1 one can see the different candidates for the acceleration of two different ions, protons, and iron. One of the candidates is the AGN, which is the focus of this paper.

The method of acceleration can be important for different sources. Here I will briefly go through some. **One-shot acceleration:** In the presence of an ordered electric field, one can continuously accelerate charged particles. This could be the feature of some astrophysical objects such as neutron stars and black holes.

Diffusive acceleration/ Fermi acceleration In regions where one has high variability in the magnetic field strength, one can accelerate particles in steps. This is called diffusive acceleration and the most common way of this happening is through first and second-order Fermi acceleration. The second-order Fermi acceleration is the simplest and is based on the fact that particles can gain energy by bouncing back and forth between magnetic clouds which act as mirrors. This is a stochastic process and the average energy gain can be shown to be proportional $(\frac{v}{c})^2$. Here v is the speed of the cloud and c is the speed of the particle. This is a slow process due to the scarcity of clouds, and therefore it is not a preferred method. The first-order Fermi acceleration happens when particles collide with strong shock fronts. These shock fronts can be quite a bit faster than the interstellar clouds and when a particle moves through the shock it gains energy proportional to $\frac{v}{c}$. In addition to this, there is a probability that the particle will stay in the accelerating region and experience several accelerations.

By knowing how particles can be accelerated and their potential sources one can continue and look at the two particles in question in this paper. Neutrinos and UHECRs.

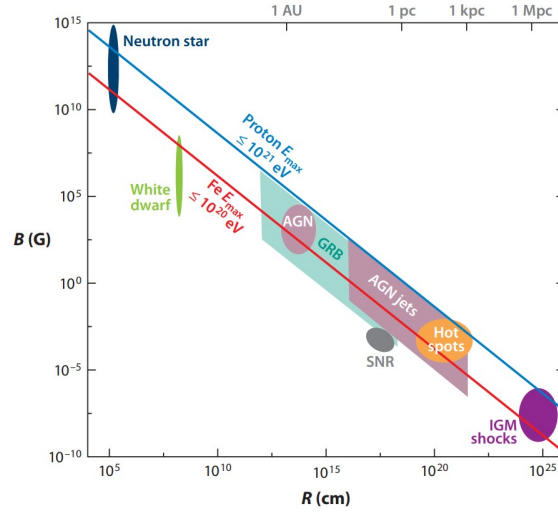


Figure 1: Hillas criterion for proton (blue line) and iron (red line) accelerated up to 10^{20} eV and 10^{21} eV respectively. Image taken from Kotera and Olinto 2011

3.2 UHECRs

UHECRs are charged particles that are bombarding the Earth with energy exceeding 1 exaelectronvolt (10^{18} eV) Alves Batista et al. 2019. The origin of these particles is still a mystery but due to their high energies, they are thought to be extragalactic in origin and due to the Hillas criterion need to be sufficiently good accelerators. The composition of UHECRs ranges from protons to heavier nuclei such as helium or iron, and when these particles interact with the atmosphere they produce a shower of secondary particles. The air showers could also give extra information such as direction, but due to the nature of UHECRs, the location of their source is difficult to pinpoint. This is because UHECRs are charged particles and therefore are deflected by the magnetic fields they encounter.

3.2.1 Production and Energy loss

The requirements to produce a UHECR are a charged particle and a powerful accelerator. But in order to model them sufficiently one needs to take into account their journey to the Earth. Both during the acceleration and during the journey to Earth, the UHECRs will lose energy. The important parameters for this energy loss are its composition and its environment. In addition, as mentioned before, the interstellar magnetic field will also deflect the particles and therefore the direction of the particle will be changed. These effects are important parameters since they limit the distance a particle can travel before its initial energy becomes unreasonably large, and therefore limits the local volume in which it can be produced. Here I will briefly discuss the different energy loss mechanisms.

Photo-pair production

$$p + \gamma \rightarrow p + e^- + e^+ \quad (10)$$

For UHECRs, the most dominant sink of energy for when at relatively low energy is the Bethe-Heitler process. In this process, a proton of sufficient energy interacts with the photon field in its vicinity and produces a pair of electrons and positrons. The photon field can vary from the cosmic microwave background to the generated field from different sources. The energy loss of this process is quite small $\sim \frac{2m_e}{m_p} = 10^{-3}$ of the original energy of the proton, but the process is very common, and therefore it is a significant energy loss over time.

Photo-Pion production

$$p + \gamma \rightarrow \Delta^+ \rightarrow (p + \pi^0) \quad \text{or} \quad (\pi^+ + n) \quad (11)$$

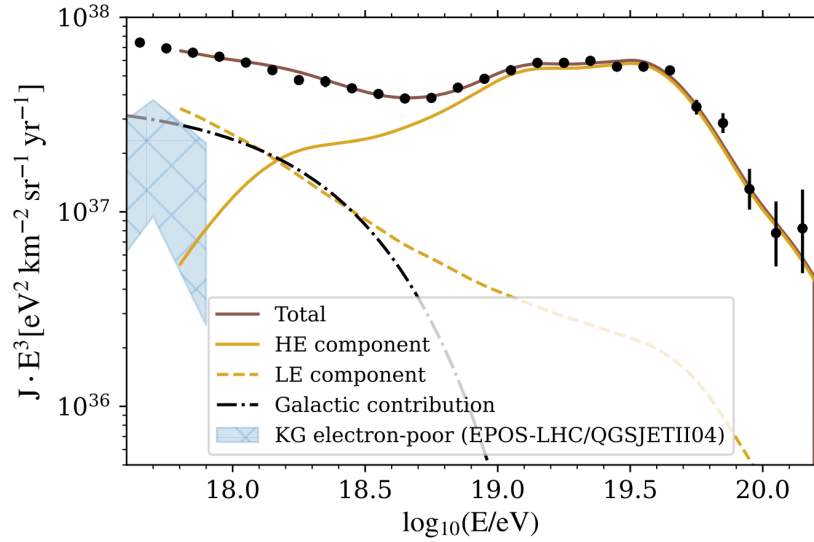


Figure 2: The diffuse flux of UHECRs as measured by the Pierre Auger Observatory and the Telescope Array. The flux is separated into galactic and extra galactic sources where the total spectrum follows the black dots. Image taken from Abdul Halim et al. 2023

Given enough energy the proton can interact with the photon field and produce a delta resonance. This resonance can then decay into a pion and a proton or a neutron and a pion. It is important since it also puts an upper limit on the UHECR energy for intergalactic particles. This limit, called the Greisen-Zatsepin-Kuzmin (GZK) limit comes from the UHECRs interacting with the cosmic microwave background in this delta resonance process. The limit caps proton energy at 5×10^{19} eV. In this mechanism the original proton loses $m_p/m_\pi \approx 20\%$ of its energy resulting in a quite rapid loss of energy.

3.2.2 Detection

When a cosmic ray hits the atmosphere it will interact with the air molecules and produce a cascade of particles and light that can more easily be detected than the original cosmic ray. In addition, since the UHECR flux at high energy is extremely low (< 1 particle per km^2 per year for $E > 10^{19}$) one needs a large area to collect enough data. The largest UHECRs detectors of present are the Pierre Auger Observatory and the Telescope Array.

The Pierre Auger Observatory is located in Argentina and is the largest detector of its kind. It consists of 1660 Cherenkov detectors spread over 3000 km^2 and 27 fluorescence telescopes in four locations. With these instruments, the observatory is very capable of reconstructing the air showers and therefore the energy and direction of the cosmic ray. The observatory has a blind spot in the night sky and therefore the observatory is complemented by the Telescope Array located in Utah. The Telescope Array is a smaller observatory with 507 scintillator detectors and 3 fluorescence telescopes. Combined they have been able to map the full sky of UHECRs.

3.2.3 Emissivity estimates

Now that one reasonably understands the nature of UHECRs one can try to make tangible estimates of the UHECR sources. One such estimate is the emissivity of UHECR sources. The emissivity is a measure of the energy released per unit time per unit volume. The question one can ask is what is the necessary emissivity of UHECRs to explain the observed flux here on Earth? In other words, what is the required energy injection rate of UHECRs?

Via observations from the Pierre Auger Observatory and the Telescope Array, one can observe and model the

diffuse flux of UHECRs. The result is an isotropic flux and is represented in Figure 2. By separating the flux into contributions from extragalactic sources and galactic sources one can estimate the required energy density in the Universe of extragalactic UHECRs. From here can define an energy loss time for a UHECR as the loss length divided by the speed of light c . The loss length is a measure of the distance a UHECR can travel before its energy drops below a certain threshold, and for our simple analysis, we will use the length of $1Gpc$. This number is comparable in magnitude as found by Stanev 2009 but as the loss length is dependent on initial energy and composition our number will be an approximation. Then the emissivity of UHECRs produced by the sources as the energy density divided by the loss time.

The previous discussion is summarized in the following equation

$$\epsilon_{\text{UHECR}} = \frac{u_{\text{UHECR}}}{t_{\text{loss}}} = \frac{u_{\text{UHECR}}}{D_{\text{loss}}/c} = \frac{4\pi c \int_{E_0}^{E_{\text{max}}} J_{\text{extragalactic}}(E) E dE}{c D_{\text{loss}}} \approx 9 \times 10^{44} \frac{\text{erg}}{\text{Mpc}^3 \text{yr}}. \quad (12)$$

Here u_{UHECR} is the energy density of UHECRs, t_{loss} is the energy loss time, D_{loss} is the loss distance, $J(E)$ is the flux of UHECRs, E_0 is the minimum energy of the flux where it is dominated by extragalactic UHECRs, and E_{max} is the maximum energy of extragalactic UHECRs. The value of ϵ_{UHECR} is calculated in the script available on GitHub Andrews 2023 by using data from Auger Collaboration et al. 2017. This emissivity is a crude estimation of the required energy injection rate of UHECRs and is meant to give a rough estimate. The main points of criticism are the estimate of our loss distance which does not include the composition of the UHECRs or its initial energy. Nevertheless, one receives an emissivity comparable to a more thorough analysis from Aab et al. 2020 which received a value of $6 \times 10^{44} \frac{\text{erg}}{\text{Mpc}^3 \text{yr}}$.

3.3 Neutrinos

The second particle of interest is the neutrino. Neutrinos compared to UHECRs are neutral particles that are produced in various processes in the Universe. The most common and well-known is the fusion reaction in the sun where neutrinos are produced in the pp chain. On the other hand the neutrinos of focus in this paper are high-energy neutrinos that are likely produced in the same sources as the UHECRs.

3.3.1 Production and Energy loss

The production sites of high-energy neutrinos is not clear, but they are thought to be produced in the same sources as UHECRs and in this section, I will go through the most probable way of producing high-energy neutrinos in sources such as AGNs.

Hadronic processes:

Hadronic processes can release neutrinos with sufficiently high energy to explain the observations here on Earth. Processes such as nuclear interactions are limited by the binding energy of the nucleus and accelerating a neutrino after its production is difficult. Therefore, a common way of producing the observed neutrinos is through the decay of pions. The most important decay is the decay of charged pions into muons and muon neutrinos as seen in 13

$$\pi^+ \rightarrow \mu^+ + \nu_\mu \rightarrow e^+ + \nu_e + \nu_\mu + \bar{\nu}_\mu \quad (13)$$

I will discuss two possible ways of producing these pions in two different environments.

In a proton-rich environment where the protons can accelerate up to high energies, one can produce pions through the following process

$$p + p \rightarrow \begin{cases} \pi^+ + n + p \\ \pi^- + \pi^+ + p + p \\ \pi^0 + p + p \end{cases} \quad (14)$$

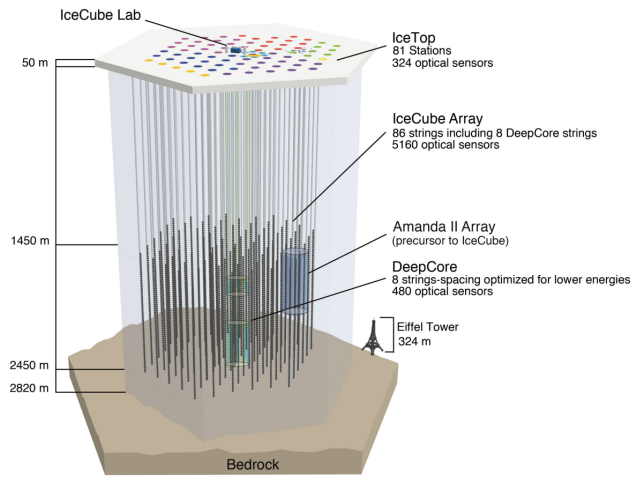


Figure 3: The IceCube neutrino observatory. The detector is located at the South Pole and is a large block of ice instrumented with photomultiplier tubes. Image taken from Andeen and Plum 2019

The energy of these protons at a few GeV is enough to introduce the delta-baryon resonance, and therefore it becomes more complicated. The most efficient way of producing pions is through the already seen delta resonance when a proton interacts with a photon ¹¹. This process being the cooling process of UHECRs above the GZK limit is interesting and indicates that a source that produces high energy neutrinos likely is inhabited by very energetic charged particles. After having produced the neutrinos it also becomes important to understand their behavior during their travel to Earth. Here I will highlight two points

Neutrino oscillations In the previous paragraph, I discussed the production of these neutrinos, but not their initial flavor. The pion decay model is known to produce a flavor composition of $\nu_e : \nu_\mu : \nu_\tau = 1 : 2 : 0$. A naive thought would be an identical composition observed on Earth, but sadly this is not the case. The reason for this is that the neutrinos' mass state can oscillate between the different flavors. Therefore, the neutrinos produced in the source will oscillate during their travel to Earth and when they reach us one would expect a uniform mix of the three flavors, $\nu_e : \nu_\mu : \nu_\tau = 1 : 1 : 1$.

Energy loss To model the travel of a neutrino of any flavor one only needs to take into account the interaction of the neutrino with the expanding universe. Since it is so weakly interacting the only source of energy loss the flux of neutrinos will experience is the redshift created by the expansion of the Universe. This redshift is the same as the one discussed in the previous section and the neutrinos behave the same way light does in this manner with a drop in energy proportional to $(1 + z)$.

3.3.2 Detection

Neutrinos are weakly interacting matter particles and therefore are very difficult to detect. This makes them excellent candidates for the study of the Universe since they can travel large distances without interacting, but make them quite difficult to detect with high accuracy. The most famous detector and the one used in this paper is the IceCube neutrino observatory. This detector is precisely what it sounds. It is a large block of ice with a size equal to a square kilometer located at the South Pole. The observatory uses the ice located deep in the South Pole as a giant Cherenkov detector. The ice is instrumented with photomultiplier tubes that can detect the Cherenkov radiation produced by neutrinos interacting with the ice. More precisely the observatory is fitted with 5160 photomultiplier tubes located at a depth of 1450-2450 m. The photomultipliers are divided into 86 strings of 60 modules each. The detector is also complemented by the DeepCore detector which is a denser array of photomultiplier tubes located in the center of the detector. See Figure 3 for a visual representation of the detector. The energy range for this detector is from 10 GeV to 10 EeV. The interaction of neutrinos with the water molecules in the ice can produce charged leptons (muons, electrons or taus). These charged particles if energetic enough will then produce Cherenkov radiation which can be detected by the photomultiplier tubes.

Φ_0	E_0	γ
$6.7 \times 10^{-18} \text{GeV}^{-1} \text{cm}^{-2} \text{s}^{-1} \text{sr}^{-1}$	100TeV	2.37

Table 1: The model parameters for the astrophysical flux of neutrinos as measured by the Ice Cube observatory.

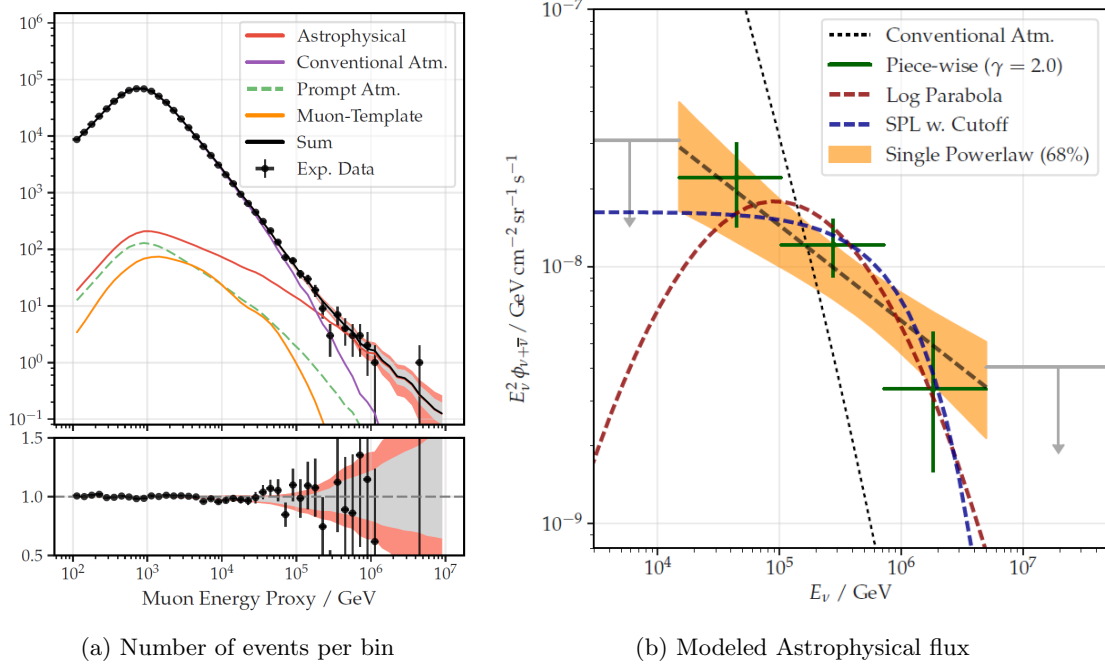


Figure 4: The diffuse flux of neutrinos as measured by the Ice Cube observatory. The y-axis on the left image is the number of events per bin. The flux is separated into contributions from atmospheric neutrinos and astrophysical neutrinos. The right image is the model astrophysical flux as measured by ICE CUBE. Images taken from Abbasi et al. 2022

3.3.3 Emissivity estimates

Armed with the required knowledge above one can also make simple arguments for the sources of these neutrinos based on the observed flux here on Earth. The flux used in this paper is the diffuse flux of neutrinos as measured by the Ice Cube observatory. The flux is shown in figure 4. For any calculations, we use the astrophysical flux as modeled as a power law. The power law is of the form

$$\Phi(E) = \Phi_0 \left(\frac{E}{E_0} \right)^{-\gamma} \quad (15)$$

with Φ_0 being the normalization constant, E_0 being the reference energy and γ being the spectral index. The model parameters are seen in table 1 and taken from Abbasi et al. 2022.

The emissivity of neutrinos is calculated in the same way as for UHECRs. The only difference is the loss time. Neutrinos do not lose energy in the same way as UHECRs and therefore the loss distance will be the size of the Universe. The modeled emissivity is then approximately $1.54 \cdot 10^{44} \text{ erg/Mpc}^3/\text{yr}$.

4 Active galactic nuclei

Active Galactic Nuclei (AGNs) are an interesting topic in astrophysical studies, and since their discovery, there has been rapid advancement in understanding these phenomena. Today, AGNs are known to be among the brightest entities in the night sky, but they only gained significant attention in the early 1950s. This shift occurred with the arrival of new radio observations, which revealed a new type of quasi-stellar object through the discovery of the Quasars.

Initially, these luminous objects, characterized by broad, unidentifiable spectral lines, were enigmatic to scientists. However, with the identification of more sources and their optical parts, it became clear that these were not stars but a distinct class of celestial objects. Furthermore, research done by M. Schmidt on one of the emission lines from Quasar 3C 273 opened the interpretation of these celestial objects. He found that the emission lines of quasars were similar to hydrogen, but were redshifted by a factor of 0.158, an exceptionally high value at the time according to Shields 1999. Observations at the same time also revealed significant variability in quasar luminosity, suggesting that these objects were no larger than one light year across. These observations lead to the speculation of super luminous objects located very far away from Earth. The problem was that such objects had no reasonable explanation at the time.

Observation of the surrounding galaxy of AGNs with matching redshift and observation of gravitational lensing cemented the distances of these objects. In addition, the modern view of black holes which had only been a theory in the 1950s came to fruition and the idea of accretion allowed for the modern model of an AGN to be born. This modern perspective views AGNs as supermassive black holes that accrete matter from surrounding gas. In addition to this the modern view of AGNs also include jets, torus, and different emitting regions that are used to classify AGNs.

In the most recent times, a landmark achievement was achieved in March 2021, when scientists associated with the Event Horizon Telescope project presented the first image of the supermassive black hole at the center of the Messier 87 galaxy, located 55 million light-years away. This image, showing a bright ring surrounding a dark central region, aligns with predictions for an accreting supermassive black hole, increasing our confidence in the modern model.

These observations made it clear that AGNs are very powerful emitters and from this the possibility of AGNs being the source of UHECRs and neutrinos was introduced.

4.1 AGN structure and classification

The modern view of AGNs is a unified model that combines the different categories of powerful luminous objects cataloged in the mid to late 20th century. These distinctions that astronomers made still have value, but to understand an AGN it is important to get a picture of the unified structure.

An active galactic nucleus is defined as a galaxy center containing a massive accreting black hole. This mass according to Netzer 2015 is defined as $M_{BH} > 10^5 M_{\odot}$. AGNs also contain an Eddington ratio exceeding the limit of $L_{AGN}/L_{Edd} = 10^{-5}$, where L_{AGN} is the bolometric luminosity, and L_{Edd} is the Eddington luminosity for a solar composition gas. These definitions help constrain what galaxies might contain an AGN, it excludes the Milky Way by these criteria, but it fails to capture the full structure definition of an AGN. Therefore, the structure of most AGNs will include several of the following components, first summarized then expanded upon:

The reader is directed to image 5 for a visual representation of the different components.

4.1.1 Accretion disk

An accretion disk is a natural consequence of the conservation of angular momentum. In the case of infalling matter coming close to a supermassive black hole, the matter could have some angular momentum. With this the gas should orbit the black hole at some stable distance but, due to radiative processes, fluid viscosity, and gravitational

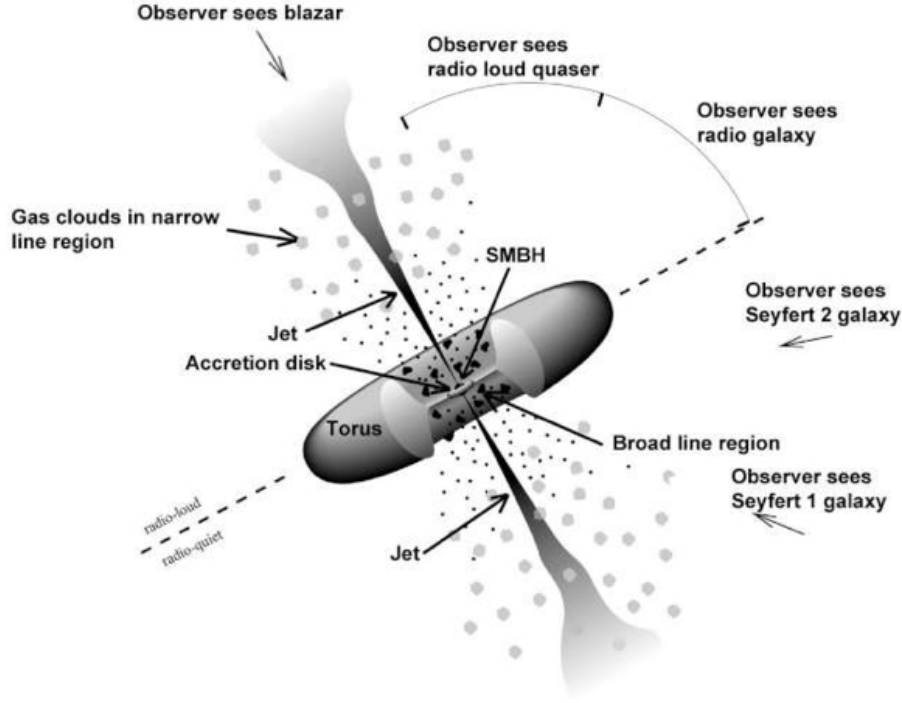


Figure 5: AGN unification

turbulence, the matter will lose angular momentum and spiral inwards. The inward spiral will eventually allow the matter to fall into the black hole. This process of inspiral is what is called accretion and the forces acting on the matter to cause the inspiral will also in the same process heat it up to high energies causing it to radiate. The radiation is closely linked to the infalling matter that is accreted onto the black hole and one can express the total luminosity of the accretion disk as

$$L_{acc} = \eta \dot{M} c^2. \quad (16)$$

Here η is the efficiency of the accretion disk, \dot{M} is the mass accretion rate and c is the speed of light.

The efficiency of the accretion disk is a function of the spin of the black hole and the radius of the innermost stable circular orbit (ISCO). The ISCO is a counter-intuitive term in classical mechanics but in general relativity the maximum speed of a particle in addition to an energy term when calculating the orbit set bounds for how close a particle can be to a black hole without spiraling in.

The accretion disk also has a bound for its maximum luminosity. As calculated for stars the Eddington luminosity sets a maximum strength for the radiation pressure of the accretion disk. This is given as

$$L_{Edd} = \frac{4\pi G M m_p c}{\sigma_T} \quad (17)$$

The heating of the accretion disk will lead to thermal radiation from the disc and this radiation will be proportional to the temperature of the disc. This temperature is radially dependent and if one assumes an optically thick but geometrically thin disk also called a Shakura-Sunuaev disk one can express the radiative surface energy flux taken from Dermer and Menon 2009(p. 106) as

$$\frac{dE}{dAdt} = F_{rad}(r) = \frac{3GM\dot{M}}{8\pi r^3} \left(1 - \beta \sqrt{\frac{r_{ISCO}}{r}}\right) \quad (18)$$

Here β is a constant that relates the fraction of angular momentum captured by the black hole, and r_{ISCO} is the radius of the innermost stable circular orbit. The temperature of the disk lie between $10^5 - 10^2$ K with emission in the optical, UV to soft X-ray range according to Abramowicz and Straub 2023.

4.1.2 Corona and X-ray emission

From highly varying x-ray observations of AGNs, it became indicative that there was a source of X-rays located close to the black hole. The most contemporary idea is that a corona of energetic particles is located above the accretion disk, and through inverse Compton scattering of the optical/UV photons that arise from the accretion disk produce the seen x-ray emission.

Inverse Compton scattering is the process of a photon gaining energy from a nearby relativistic particle. Due to the increase in efficiency of up scattering a photon with an electron compared to a proton, the corona x-ray emission is thought to be dominated by electrons. The process is as follows

$$e^- + \gamma \rightarrow e^- + \gamma \quad (19)$$

The reason of interest for this area is that the correlation between the produced x-ray luminosity can possibly be used to infer some luminosity of the more elusive particles UHECRs and neutrinos. A simple argument for this is that the ingredients for this x-ray production are the same as for the production of UHECRs and neutrinos (charged particles). In addition, the acceleration into the jet-like structure as shown by of AGN needs a source of particles and the corona is a natural candidate for this.

4.1.3 Broad and narrow line region

Broad emission lines in the case of AGN are formed from the high-density gas clouds located close to the central black hole. The high-density parameter is inferred from the fact that one only sees broad emission from permitted line transitions (f.ex hydrogen Lyman and Balmer, iron II, and magnesium II). High densities allow for collisional de-excitation and in doing so prohibit so-called forbidden transitions. The broadening is an indication that these gas clouds are moving at huge velocities around the massive objects. This implies that they are located close to the black hole and receive the name the broad line region

Narrow emission lines are on the other hand formed in low-density gas clouds. The low densities are inferred from the fact that one sees both permitted and forbidden line transitions. They are narrow lines due to their velocities being substantially lower than the innermost gas clouds, and from here are thought to be located further away from the black hole, in the narrow line region.

4.1.4 Dust torus

The dust torus is a structure of dust that is thought to be located quite close to the black hole (0.1 - 10 pc). The main argument for the existence of this structure is the obscuration of the central region of the AGN. This obscuration is part of the unification scheme of AGNs and was backed by the detection of polarized broad lines in AGNs with their central core obscured. This polarization is what we would expect if some dust was obscuring the central region since the only light one sees is the light that is scattered into the line of sight Mason 2015. Further, studies on the dust torus have also revealed that the torus is not uniform but clumpy and quite dynamic with both in and outflows of matter depending on the state of the central engine Mason 2015.

4.1.5 Jets

A jet is a highly collimated outflow of plasma. The origin of the plasma is thought to be the accretion disk and the hot corona above it. These regions that have a high density of charged particles will under the influence of a

magnetic field be accelerated and collimated into a jet-like structure. The energy mechanism which powers the jet is not fully understood, but the most prevalent theory is the Blandford-Znajek process. It says that the rotation of the accretion disk induces a magnetic field that will interact with a rotating black hole, effectively extracting energy from the black hole and supplying it to the jet. The jet structure extends far beyond the local area of the AGN maintaining a stable configuration over these distances. The classification of these jets is usually divided into two groups according to Walg et al. 2013, FRI and FRII. They are differentiated by their luminosity where FRI jets are less luminous and have a more diffuse structure while FRII jets are more luminous and have a more stable structure reaching further out. To add to this distinction it is thought that FRII jets are a product of an efficient accretion disk while FRI jets are a product of an inefficient accretion disk. This is discussed in Bian and Zhao 2003 where they show that radio quiet and Seyfert 1 galaxies have lower accretion efficiency while radio loud galaxies have higher accretion efficiency. Beyond the energy and their structure, the jets are also notable for their emission of non-thermal radiation such as synchrotron and inverse Compton radiation.

4.2 Types of AGNs

Before the unification of the AGNs astronomers named the puzzling objects based on their observational properties. These names are still used to this day and are somewhat useful since their observational properties are important parameters for further study. The different classifications are important in understanding which objects could have the potential to produce the different observables one looks for in the night sky. Therefore, it seems appropriate to discuss some different types of AGNs and their observational properties. The classification in this section is heavily based on Sanders 2021.

Type I and II AGNs: One distinguishes type I and type II AGNs based on the presence of broad emission lines. In other words, this distinction is a matter of a visible nucleus or not. Type I refers to sources whose nucleus is exposed to the observer and whose spectrum has both narrow and broad emission lines. Type II refers to sources whose nucleus is obscured by a torus and therefore mainly has narrow emission lines.

Blazars: The most extreme class of AGN. These sources are distinguished by their relativistic jets that are pointed towards the observer. This jet produces both synchrotron and Inverse Compton gamma rays and are extremely variable over short timescales. The emission is also highly polarized. Often and including in this report one divides Blazars into subgroups based on the emission lines. The two most common are BL Lacs and Flat spectrum radio quasars (FSRQs). The difference between the two is the presence of broad emission lines, where BL Lacs have no broad emission lines while FSRQs do. In addition, the distinction comes from the type of jet structure thought to be associated with the source. FRI jets for BL Lacs and FRII for FSRQs.

Radio galaxies: As the name suggests these sources are very bright in the radio band. They usually refer to AGN viewed edge-on, where the torus might block the emissions from the accretion disk. The orientation of Radio galaxies gives way to strong synchrotron radiation, and they are often used to study the jet structure of AGNs.

Seyfert galaxies: Spiral galaxies that have a bright nucleus. They are bright in the optical band and have a smaller active region than radio galaxies. They are often divided into two groups Seyfert I and Seyfert II where the distinction comes from type I and II. The galaxies also show quite high variability indicating a small emitting region.

Compton thin AGNs: A way of distinguishing AGNs that can be quite useful. These AGNs have lower absorption compared to Compton-thick AGNs, which allow more X-rays to escape making them easier to identify.

All these different distinctions are a help in understanding what processes one might be observing. The different dominant bands indicate different processes being in the line of sight, and by considering the modern structure of AGNs one can then try to determine the underlying dynamics.

5 Luminosity functions

In this section, we will discuss the use of luminosity functions to characterize the populations of different AGNs. A luminosity function (LF) is a function that maps the distribution of celestial bodies, like galaxies or quasars, based on their luminosity and corresponding comoving volume elements. These functions serve as a tool to understand the evolutionary patterns of these objects and allow us to predict the number density of these objects.

Typically, the focus is on the differential luminosity function, which is defined as

$$\frac{d\Psi(L, z)}{dL} = \frac{d^2 N(L, V_c(z))}{dL dV_c(z)}. \quad (20)$$

One also can change the differential of the comoving volume into a term only depending on the redshift assuming the source population is isotropic and by multiplying with the differential comoving volume element. This transformation goes as follows,

$$\frac{d^2 N(L, V_c(z))}{dL dV_c(z)} \frac{dV_c(z)}{dz} = \frac{N(L, z)}{dL dz}. \quad (21)$$

Several articles express the luminosity function in base 10 logarithm, and we note the conversion between the two:

$$\frac{d\Psi(L, z)}{d\text{Log}(L)} = \ln(10) L x \frac{d\Psi(L, z)}{d(L)}. \quad (22)$$

To effectively determine the LF, it's typically divided into two distinct components: a local term and a time evolution term. This approach involves taking the local luminosity function, calculated at a redshift $z = 0$, and then scaling it with a function that accounts for the redshift evolution. The exact form of the total LF varies based on the source object, but it generally falls into two categories derived from the method of incorporating the evolution term into the local LF. These methods are selected based on which best represents the observed evolution.

The two distinctions are the Pure Density Evolution (PDE) and the Pure Luminosity Evolution (PLE). The PDE model modifies the local density function to reflect changes over time, while the PLE model adjusts the local luminosity. The evolution is better represented by their equations and is given as

$$\frac{d\Psi(L, z)}{d(L)} = \begin{cases} \frac{d\Psi(L/e(z), z=0)}{d(L)} & (PLE) \\ \frac{d\Psi(L, z=0)}{d(L)} e(z) & (PDE) \end{cases}. \quad (23)$$

Here one sees the common way of representing the luminosity functions. The local luminosity function is scaled by a factor of $e(z)$ which is the evolution term.

5.1 X-ray LF

For a given type of celestial object, different spectral bands will be more useful than others. In the case of AGNs, the X-ray band is particularly significant. Therefore, several studies have focused on defining the luminosity functions of AGNs with the X-ray spectrum.

In the following, I will define the x-ray luminosity functions for various AGN classifications, including Radio Galaxies, Seyfert Galaxies, and Blazars. Furthermore, an additional breakdown will consider FSRQs and BL Lacs within Blazars. In addition to this, a study by BUeda et al. 2014 also looked at the total evolution of all Compton-thin AGNs by combining multiple surveys and research. It will work as a reference point as well as describe the total evolution of these objects. The luminosity functions are collected from three papers Ajello et al. 2009 and Silverman et al. 2008, and BUeda et al. 2014 and their form is explained below.

Parameter values for the X-ray luminosity functions

Model	LF params				Evolution params				
	A	L_{star}	γ_1	γ_2	v_1	v_2	z_c	L_c	α
SLDDE RG	8.375 ^a	2.138 ^b	2.15	1.10	4.00	-1.50	1.90	3.981 ^b	0.317
AMPLE-Blazar	1.379 ^a	1.810 ^b	-0.87	2.73	3.45	-0.25			
AMPLE-FSRQ	0.175 ^a	2.420 ^b	-50.00	2.49	3.67	-0.30			
APLE-BLlac	0.830 ^a	1.000 ^b	2.61		-0.79				
APLE-Seyfert	0.909 ^b	0.61 ^b	0.8	2.67					
ULDDE-CTN AGN ^c	2.91 ^a	0.93 ^b	0.96	2.71	4.78	-1.5	1.86	4.07 ^b	0.29

Table 2: X-ray LF parameters, a , normalized by a factor of 10^{-7} , b , normalized by a factor of 10^{44} c , has more factors that do not fit in the table, $z_{c2} = 3$, $\alpha_2 = -0.1$, $L_{c2} = 10^{44}$, $v_3 = -6.2$, $\beta = 0.84$

Model Name	Luminosity Range (Log(L))
SLDDE RG	42 - 47
AMPLE Blazar	43 - 49
AMPLE FSRQ	45.5 - 49
APLE BLlac	44.5 - 49
APLE Seyfert	41 - 47
ULDDE All CTN AGN	42 - 46

Table 3: Luminosity range for different models

The local luminosity function:

The local luminosity function is the luminosity function at $z = 0$. The simplest form of the local luminosity function is expressed in Ajello et al. 2009 and is given as a power law. For our classes, it represents only the local LF for the class of BL Lacs and is given as

$$\frac{d\Psi(L, z = 0)}{dL} = \frac{A}{L_x} \left(\frac{L_x}{L_*} \right)^{1-\gamma_2} \quad (24)$$

This functional form has the fewest parameters and therefore suits well for populations that have few detected sources, but has the disadvantage of not being able to capture all the details of the observed local luminosity functions when source counts increase. For that reason a more complex local function is needed which was proposed in Ueda et al. 2003 and is described by a double power law. The double power law is used for the remaining classes of AGN and is given as follows

$$\frac{d\Psi(L, z = 0)}{dL} = \frac{A}{\log(10)} \frac{1}{L_x} \left(\left(\frac{L_x}{L_*} \right)^{\gamma_1} + \left(\frac{L_x}{L_*} \right)^{\gamma_2} \right)^{-1} \quad (25)$$

Evolution factor:

In addition to the local LF one also considers the evolution factor denoted $e(z)$. This factor captures the observed evolution of these objects and is the second part of the total luminosity function.

Again for the simplest evolution with the fewest parameters, a power law is used.

$$e(z) = (1 + z)^{v_1}$$

Certain situations necessitate a more detailed approach to the redshift evolution. As detailed in Ajello et al. 2009, a modified evolution is frequently employed. This adaptation transforms the conventional Pure Luminosity Evolution (PLE) and Pure Density Evolution (PDE) into their modified counterparts, namely Modified PLE (MPLE) and

Modified PDE (MPDE). It is within these modified frameworks that a dependence on redshift z emerges in the exponent, providing a more nuanced understanding of the evolutionary processes involved. It is given as

$$e(z) = (1 + z)^{v_1 + v_2 z}$$

To expand further as described in Silverman et al. 2008 the evolution factor of the luminosity function is not always as simple as a modified power law only dependent on the redshift z . For some sources, a more complex evolution is needed. In Silverman et al. 2008 they use a double power law to better fit the data where the evolution is now not only dependent on the redshift but also on the luminosity. This then receives the apt name as a luminosity-dependent density evolution (LDDE) since it is a modified version of a (PDE) The functional form of the LDDE is as follows

$$e_z(z, L) = \begin{cases} (1 + z)^{v_1} & \text{when } z \leq z_*(L) \\ e_z(z_*(L), L) \times \left(\frac{1+z}{1+z_*(L)} \right)^{v_2} & \text{when } z > z_*(L). \end{cases} \quad (26)$$

with $z(L)$ being defined as

$$z_*(L) = \begin{cases} z_c \left(\frac{L}{L_c} \right)^\alpha & \text{when } L \leq L_c \\ z_c & \text{when } L > L_c. \end{cases} \quad (27)$$

The expansion of the parameter space allows for easier fitting to the observed data, but comes of course with an increase in complexity and possible over fitting.

Lastly BUeda et al. 2014 considered an XLF for the entire population of AGNs and naturally this has a more complex evolution structure. It is also an LDDE model but with three steps instead of two which we have in Silverman et al. 2008. The evolution is given as

$$e_z(z, L) = \begin{cases} (1 + z)^{p_1} & \text{when } z \leq z_*(L) \\ (1 + z_*)^{p_1} \left(\frac{1+z}{1+z_*(L)} \right)^{v_2} & \text{when } z > z_*(L) \\ (1 + z_*)^{p_1} \left(\frac{1+z_{*2}}{1+z_*} \right)^{v_2} \left(\frac{1+z}{1+z_{*2}} \right)^{v_3} & \text{when } z > z_{*2}(L) \end{cases} \quad (28)$$

with the exponent p_1 being defined as

$$p_1 = v_1 + \beta(\log(L) - 44) \quad (29)$$

with $z_*(L)$ being defined as

$$z_*(L) = \begin{cases} z_c \left(\frac{L}{L_c} \right)^\alpha & \text{when } L \leq L_c \\ z_c & \text{when } L > L_c \end{cases} \quad (30)$$

and $z_{*2}(L)$ being defined as

$$z_{*2}(L) = \begin{cases} z_{c2} \left(\frac{L}{L_{c2}} \right)^{\alpha_2} & \text{when } L \leq L_{c2} \\ z_{c2} & \text{when } L > L_{c2} \end{cases} \quad (31)$$

Armed with the functional form of the total luminosity function one can now fit the parameters to the observed data. This is done in Silverman et al. 2008, Ajello et al. 2009 and BUeda et al. 2014 and their model name is a combination of the source paper (S, A, U), the type of model it describes (PLE, MPLE, LDDE) and the object in

question. The parameters are then fitted to the data using a maximum likelihood method and the observational data of several x-ray surveys, see the cited papers for more information. One can see the parameters for the different models in table 2 and the luminosity range for which the different models are valid in table 3.

6 Evolution

In this section, we will be using the different luminosity functions from the previous section to calculate the evolution of the different classes of AGNs. By understanding these trends one can start understanding the nature of these objects, when and **possibly how** they are created, and the amount of energy they release into the Universe.

6.1 Luminosity distribution

For the different classes discussed one can integrate the differential luminosity function over redshift to retrieve the Luminosity distribution of each object. This distribution highlights the difference in emitting power and therefore is important for us to be able to distinguish the most powerful sources and their prevalence, and also any trends that might be interesting. One calculates the Luminosity density by multiplying the class-specific luminosity function with the differential comoving volume and integrating over the relevant redshift bin.

The luminosity distribution is given as

$$\frac{dN(L)}{dL} = \int_{z_{\min}}^{z_{\max}} \frac{\Psi(L, V(z))}{dL} \frac{dV(z)}{dz} dz \quad (32)$$

Here, z_{\min} and z_{\max} are the limits of the redshift bin. By separating it into bins of redshift one can assess how the class varies with redshift, and how a change in redshift would change the slope/trend of the distribution.

In figure 6 one can see the luminosity density for the six different luminosity functions. The distribution is separated into four bins of redshift ($0 < z < 2$, $2 < z < 4$, $4 < z < 6$, $6 < z < 8$). The most interesting feature of these distributions is the difference between the break luminosity between jet-dominated classes such as Blazars and non-jet-dominated classes such as radio galaxies and Seyferts. For the jet-dominated ones the luminosity distribution breaks at a certain point and decreases on both sides. The only exception to this is the BL Lacs which are represented as a simple power law and therefore have no break point in their distribution. With the inclusion of more BL Lacs in future data sets it would be interesting to see if this is still the case. The breakpoint for Blazars and FSRQs indicates some preferred luminosity in which one finds the most sources. This preferred luminosity also seems consistent with different epochs. To investigate this preferred energy range one could investigate different optical bands and see if the same trend is observed. In Narumoto and Totani 2006 they also discuss the luminosity function for Blazars but in the gamma ray band. The evolution function they use is a luminosity dependent density evolution similar to our radio galaxies and CTN AGNs. They also find a peak in the luminosity distribution, this time at a higher luminosity than the one found here. Therefore, it could be that there is a distribution of Blazars around a certain total luminosity since one sees this trend in the x-ray and gamma ray band. This is not necessarily true, and one should investigate the surveys used to see the correlation between x-ray and gamma ray luminosity.

From the unified model of AGN one would not expect this correlation to be negative due to the different emitting regions.

For the non-jet-dominated classes, one sees an increase in numbers towards lower energies, but at some specific luminosity radio galaxies and CTN AGN introduce a break. The break luminosity is very interesting and differentiate itself from jet-dominated AGN since it seems to show a breaking point where the creation of more powerful sources becomes significantly harder and therefore less numerous. This breakpoint is also varying based on the redshift bin, where for higher redshift, the break is more sudden. For the Seyferts that have no evolution factor there is no distinction between lower or higher redshift. Any change in the slope of a power-law is cause for investigation since it seems to indicate some change in possibly the structure of the sources. The softening of the break depending on redshift might indicate that this break is not as sudden as one would assume looking at higher redshift objects, but the change in slope index is still observed. The different interpretation of the luminosity distribution of these objects is fascinating and further study could illuminate why one would observe this difference, and if it is an effect of the sources, our observation of them or not an effect at all. One notes these different reasons because the author of this paper has not found any explanation to why the number of our sources suddenly drop at a certain luminosity.

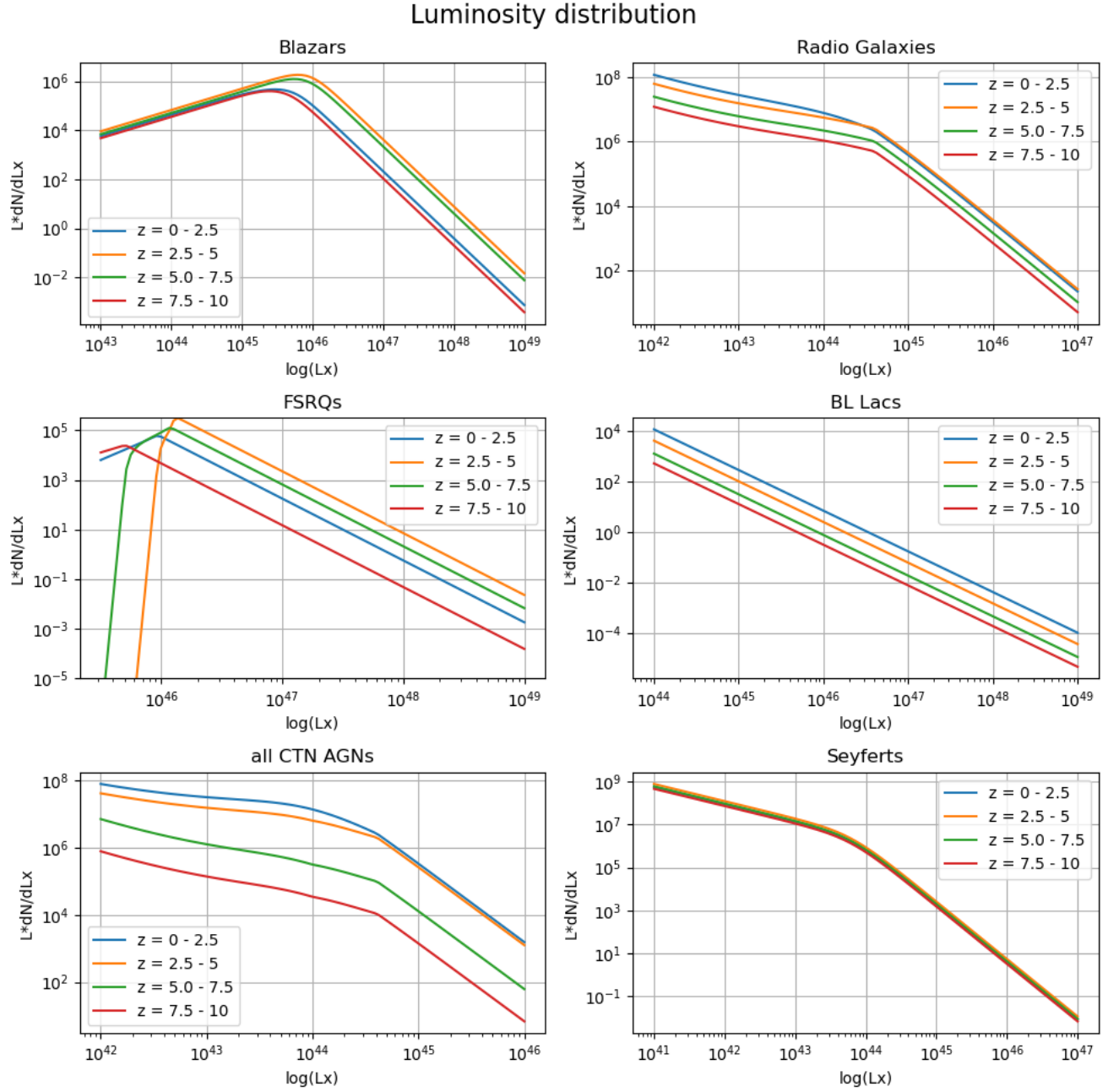


Figure 6: Luminosity density for the different classes of AGNs. The different classes are defined in the title as well as the chosen LF model.

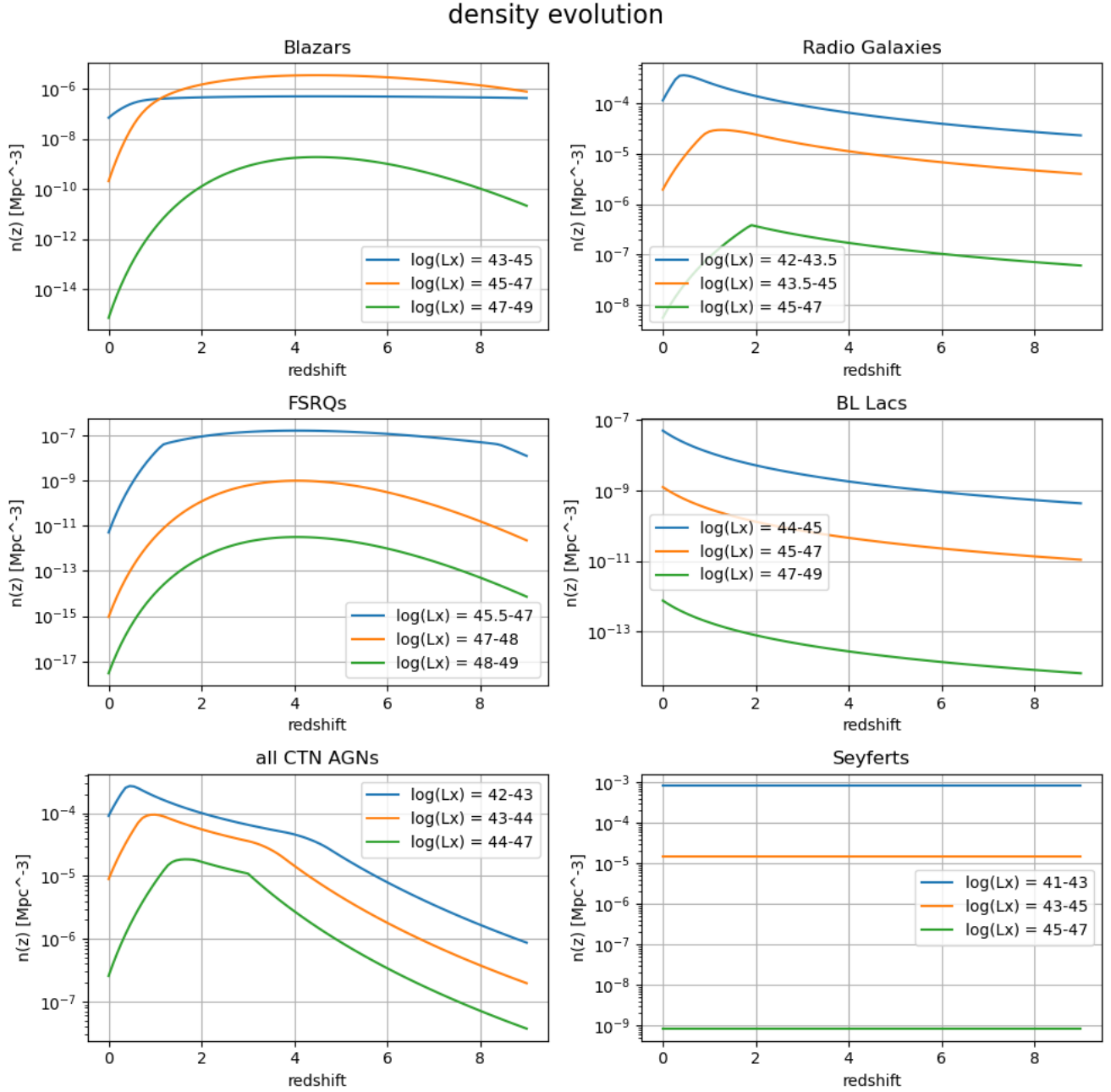


Figure 7: Density distribution for the four different classes of AGNs. The different classes are defined in the title as well as the chosen LF model.

6.2 Density distribution

In addition to the luminosity distribution one can also calculate the number density of the different classes of AGNs. This is done by integrating the differential luminosity function over luminosity. This will illuminate the evolution in time, or more precisely in redshift of the different classes. The integral is given as

$$n(z) = \frac{N(z)}{V(z)} = \int_{L_{\min}}^{L_{\max}} \frac{\Psi(L, V(z))}{dL} dL \quad (33)$$

Here again, we separate into luminosity bins to see the evolution of different parts of the luminosity distribution, most notably to see the difference before and after the break luminosity for most classes. The results can be seen in figure 7

The density evolution of these objects is very interesting information due to it being closely tied to galaxy evolution. The evolution of Blazars and FSRQs differentiate themselves significantly from the other classes in figure 7 where both FSRQs and Blazars have a positive evolution with a peak in density around redshift $z = 5$. The total counterpart to this is the third class of jet-dominated AGN, the BL Lacs. Here one sees a negative evolution with an increase in density in the more recent epochs. In a paper by Garofalo et al. 2019 he talks about the different evolutionary paths that generate the respective classes of BL lacs and FSRQs which could be the origin of this discrepancy. While both classes belong to the parent class of Blazars the evolutionary path of FSRQs is thought to come from FRII radio galaxies while the evolutionary path of BL Lacs is from FRI radio galaxies. As mentioned in section 4.1.5 the difference between FRI and FRII jets is thought to be the accretion efficiency. In addition to this a paper by Bian and Zhao 2003 which studied the correlation between accretion rates and bolometric luminosity mentions that the nature of the central black hole and its rotation will have an effect on the accretion rate. Drawing from this one could indicate that the difference in evolution stems from the different evolutionary paths of their central engine, Kerr black hole or not. This is for the time being not an accepted explanation and still a topic of debate. Another try to explain how accretion efficiency is related to the central engine is in Raimundo et al. 2012 where they discuss a finding that showed the efficiency of the accretion being proportional to the mass of the black hole. More precisely they found this relation: $\eta \propto M^{0.5}$. Although this could help explain our density evolution of FSRQs and BL Lacs by allowing FSRQs to host bigger black holes they also mentioned that this effect might be an artifact of the parameter space used. On the other hand one could also try to look at the evolution of material that can be accreted around the central black hole to possibly start unraveling the different evolutionary paths. From this it is only reasonable to conclude that this difference in evolution is captivating and is prone to an interesting answer.

For the Blazar population, one notices the same trend as for the luminosity distribution. The luminosity bin before the break luminosity stays more constant than the ones after the break. The reason for such an evolution would likely be tied to the same mechanism driving BL lacs and FSRQs. Due to the decline of FSRQs, one should also expect the higher-end luminosity of Blazars to follow.

For the non-jet-dominated AGNs, one finds a different story. Here the redshift peak, if any, is at around $z = 0.3$ where the peak is dependent on the luminosity bin. Lower luminosity AGN peaks at lower redshift. Therefore, the trend of density seems to be going toward lower-power radio galaxies and Compton-thin AGNs. What is very interesting is comparing this evolution to the evolution of star formation. From Madau and Dickinson 2014 the star formation rate peaks at around 3.5 billion years after the Big Bang, or around redshift $z = 1.9$. This is in stark contrast to our sources where only the most luminous radio galaxies and Compton thin AGNs peak at this redshift. The star formation rate then places itself in between the two peaks between jet-dominated and non-jet-dominated AGNs which opens up for interpretation.

6.3 Expected luminosity

From the luminosity function, one can also calculate the expected luminosity of a source class at different redshifts. This is important since it will directly relate to the power injection of the different epochs and from this one can calculate an expected emissivity of the different classes of AGNs. The expected luminosity of each group can be calculated with the following formula

$$\langle L \rangle = \frac{\int_{L_{\min}}^{L_{\max}} L \frac{\Psi(L, V(z))}{dL} \frac{dV(z)}{dz} dL}{\int_{L_{\min}}^{L_{\max}} \frac{\Psi(L, V(z))}{dL} \frac{dV(z)}{dz} dL} \quad (34)$$

furthermore, the emissivity is given as

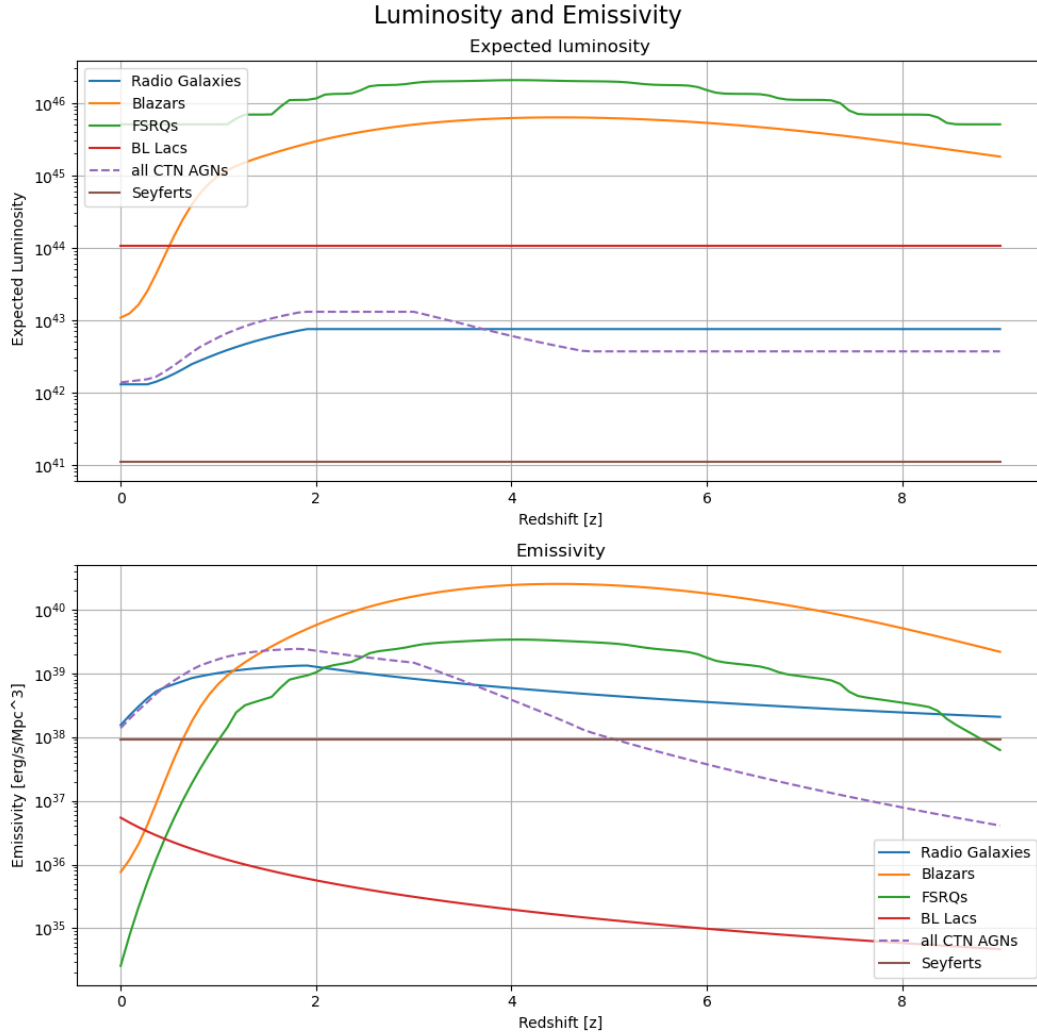


Figure 8: Expected luminosity and emissivity for the four different classes of AGNs. The different classes are defined in the title as well as the chosen LF model.

$$\epsilon = \int_{L_{\min}}^{L_{\max}} L \frac{\Psi(L, V(z))}{dL} \frac{dV(z)}{dz} dL \quad (35)$$

The different luminosity ranges are the same as before and are given in table 3. The results are shown in figure 8.

The expected luminosity is shown at the top in figure 8 where it shows the expected power output of the different classes. Here one sees that FSRQs are indeed the most luminous AGN and that they represent some of the most luminous objects in the Universe. The expected luminosity also shows the evolutionary trend of Blazars where they are now tending towards lower average luminosity. All classes remain fairly constant, but radio galaxies and CTN AGNs both have a decline in expected luminosity after the star formation peak at $z = 1.9$. This could be inferred from figure 7 but is more clearly seen here.

The emissivity of each class as a function of redshift is shown in figure 8 at the bottom. Here it shows a change in dominance between Blazars and our CTN and radio galaxies. This change that happens around redshift $z = 1$ is a result of the different evolutionary paths of our sources seen in figure 7 and should affect the diffuse astrophysical flux of UHECRs and neutrinos. Due to the different orientations of the sources one should expect them to create UHECRs and neutrinos differently. From this any decline in emissivity of for example Blazars would separate the expected flux of neutrinos and UHECRs if they are produced in the same source. This is due to the energy loss

mechanisms discussed in section 3.2.3. In order to test this one would need a way of correlating the production of neutrinos with UHECRs, and this requires to model the different ways of not only accelerating particles but also the direction of acceleration. Two possible ways of accelerating particles which compliments the different classes discussed in this report is the Blandford-Znajek process which produces jets, and outflow mechanics which can in theory take any direction but are usually discussed as outflows into the plane of the host galaxy. For jet-dominated AGNs the most accepted theory of energy extraction from rotating black holes is discussed in Blandford and Znajek 1977. This method of acceleration which is produced by ordered electric fields drives the accelerated particles into jets. One cares about this since any emission of particles especially neutrinos would therefore be highly pointed and one would only expect AGNs with a jet pointed in our line of site to produce neutrinos we would detect. The method of outflows discussed in Laha et al. 2021 is another way of accelerating particles and is akin of reconnection events that happen in the sun. The problem one faces here is therefore the uncertainty of accelerating our particles enough. The mechanism of outflow is not certain enough to produce the highest energy UHECRs and neutrinos. The orientation of these outflows can be also be difficult to determine therefore it becomes harder to use these outflows as consistent methods of generating our desired particles. These different ways of accelerating our particles are important to consider later when talking about the diffuse flux of UHECRs and neutrinos since they would be quite dependent on the class of AGN.

A note for Foteini: The last paragraph is in my opinion important, but I find it awkwardly placed, and - I feel like I do not know enough to keep it in, please correct me if I have written anything wrong or weird.

7 Energy budget estimation

7.1 UHECRs emissivity

With the calculated emissivity for the different groups, and the discussion on acceleration there is now the possibility to look from an energy budget viewpoint into the possibility of AGNs being the origin of UHECRs. By ignoring the method of acceleration, but considering that our sources must produce the required emissivity one can make a crude estimation of source candidates.

From the calculation in 3.2.3 the emissivity of UHECRs is given as $1.73 \cdot 10^{44} \text{ erg/Mpc}^3/\text{yr}$ this was calculated from the observed flux of UHECRs from the Pierre Auger observatory Collaboration et al. 2017. In this calculation, one needed to confine the area in which these sources could be produced to take into account the energy losses these particles experience. The same argument must be used for our emitting sources and therefore one must use the emissivity of our sources at a redshift very close to Earth. To get a comparable emissivity one evaluates therefore the emissivity at redshift $z = 0.01$. The result is shown in figure 2

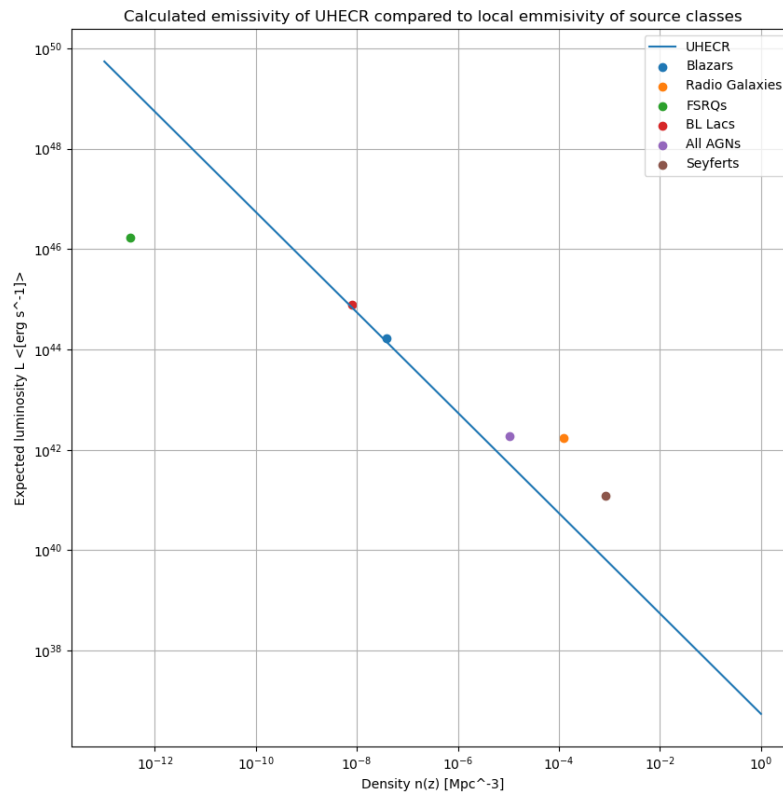


Figure 9: UHECR emissivity for the four different classes of AGNs.

This figure shows that most classes of AGN produce a total emissivity in X-ray comparable to the one energy detected by the Pierre Auger observatory. The only exception is the FSRQs which are not numerous enough at this redshift. To criticize this very crude estimate, one must first note that the correlation between X-ray luminosity and UHECR luminosity is not well-defined and should include parameters that are not accounted for. In addition to this one has not done any separation between jet-dominated and non-jet-dominated AGNs, and even though our non-jet-dominated AGNs are capable of producing the required x-ray luminosity the mechanism of transferring this energy into UHECRs as talked about in section 6.3 is not well understood.

Nevertheless, the result does not rule out the possibility of AGNs being the origin of the UHECR diffuse flux.

7.2 Neutrino emissivity

Similarly, for the UHECRs, we calculated the local emissivity for the neutrinos in section 3.2.3. The result was $1.2 \cdot 10^{44} \text{erg/Mpc}^3/\text{yr}$ which is a factor similar to that of UHECRs. In the calculation, the diffuse neutrino flux on Earth was taken from the IceCube observatory Abbasi et al. 2022 and the energy range was taken to be $1\text{TeV} - 10\text{PeV}$ corresponding to the astrophysical neutrino flux. The difference between the UHECR flux to the neutrino flux is the energy loss mechanism. The effect of a very limited energy loss mechanism means that the emitting area is now the whole universe. To reach a comparable emissivity one must therefore take a redshift-dependent average of the sources over the whole universe. One does this by scaling the emissivity at redshift z with the corresponding energy loss for a neutrino from that redshift given as $(1+z)$ and then taking the average emissivity to get a comparable emissivity. The resulting figure is shown in figure 10.

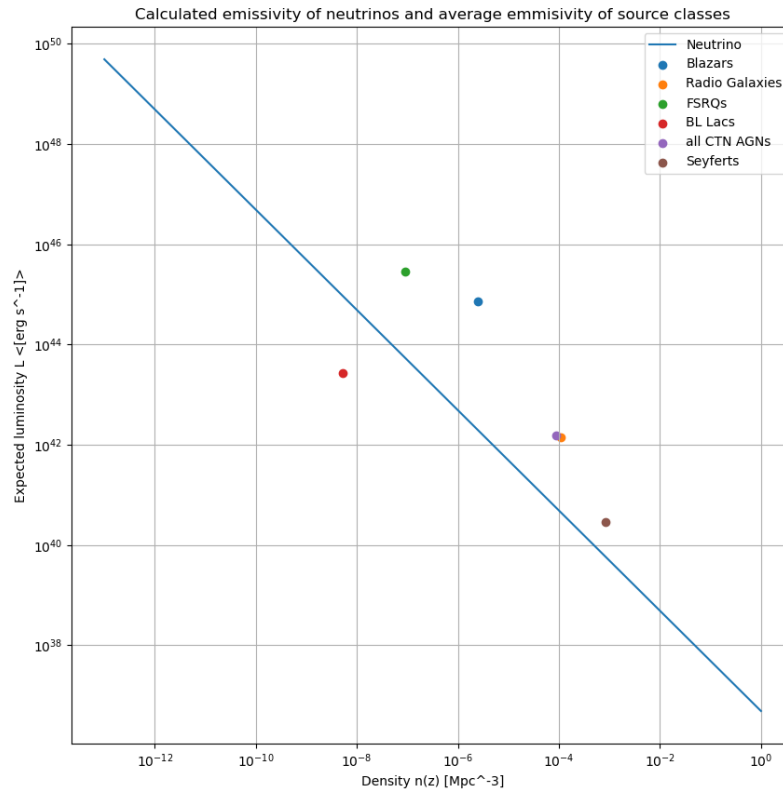


Figure 10: Neutrino emissivity for the four different classes of AGNs.

This figure shows that the neutrino flux can be produced by all classes except the BL Lacs. This is an effect of the averaging since the BL lacs have a negative evolution. The opposite is the FSRQs which now can produce the required emissivity.

In addition to the average picture given in figure 10 one can also calculate the diffuse neutrino flux directly from the different classes of AGNs. This is done by modifying the transfer function defined in Palladino et al. 2020 and this is given as

$$\frac{d\phi_\nu}{dE_\nu} = \int_0^{z_{max}} \frac{D_H}{E(z)} \frac{L(E_\nu(1+z), \langle L_x \rangle(z))}{(1+z)^2} \rho(z) dz \quad (36)$$

Here D_H is the Hubble distance, $E(z)$ is the function defined in section 2.4, $L(E_\nu(1+z), \langle L_x \rangle(z))$ is a power law representing the neutrino flux at the source, which when integrated reproduces the average source luminosity at redshift z , and $\rho(z)$ is the number density of the sources at redshift z . With this function, we can calculate the expected diffuse flux of neutrinos from the sources. The difference between Palladino et al. 2020 and I, is the inclusion of a luminosity dependence in the power-law function. This is done to account for the different average luminosity of the different classes of AGNs which was assumed constant in Palladino et al. 2020. The assumption of a constant luminosity is not a bad one since the luminosity of the different classes is not changing significantly over the redshift range, but it is still a simplification, especially for the Blazar class. The form of the spectra is taken to be identical to the observed neutrino flux by ICE CUBE which is defined in section 3.3.3. The result is shown in figure 11.

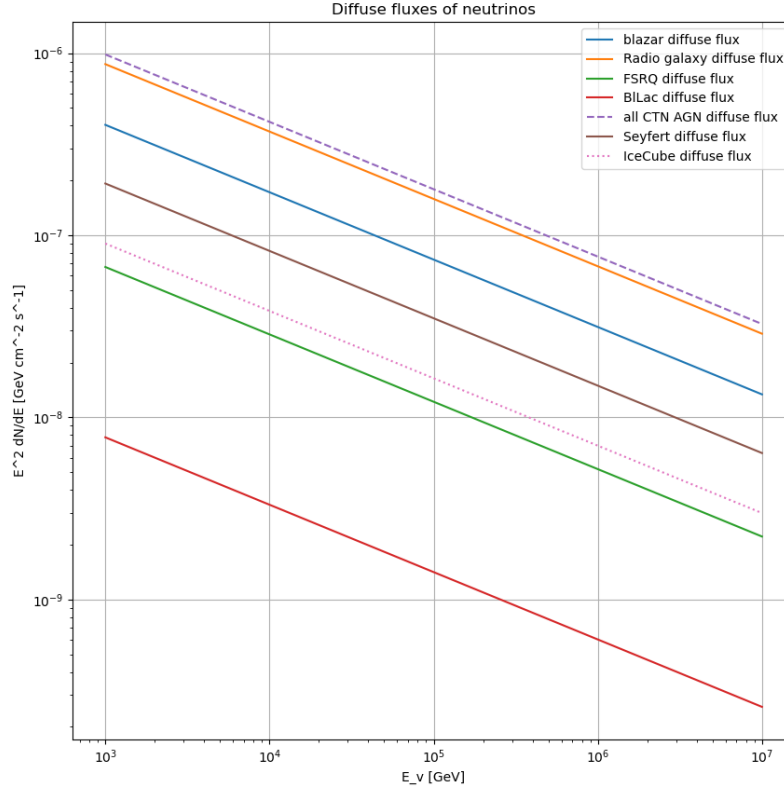


Figure 11: Diffuse neutrino flux for the four different classes of AGNs.

What one sees here is almost the same result as the crude average which is good. The FSRQs and BL lacs are now not able to produce the diffuse flux but the rest are. The fact that all sources are overshooting the observed neutrino flux would be a problem if we had a more constrained solution. Any model that overshoots could not be the source since it is not what we observe, but in our case, our solution rests on the fact that the neutrino luminosity is equal to the x-ray, an assumption easily broken and without nuance. Therefore, the only concrete conclusion one can draw from this is that the neutrino flux can be produced by the AGNs since they can produce the required emissivity. Several papers such as Kurahashi, Murase, and Santander 2022 talk about the lack of any anisotropy in the observed diffuse neutrino flux. Such an anisotropy would introduce a required density of sources. This would be a problem for the more obscure sources such as FSRQs and could further limit our predictions.

This result in figure 4 is obtained differently than in figure 10 and therefore the agreement between them is a good sign. The argument that the x-ray luminosity should have the same value as the neutrino luminosity is not a bad first guess, but it does leave a lot to be desired. This flux model does not incorporate any parameters of the AGN other than emitting strength, and therefore it is not a very nuanced model. A first fix could be a model that includes the jet orientation and most importantly the acceleration mechanism one could imagine happening. What this crude model can show is that these objects do produce enough power. To make the estimation better without doing much more work, one could look at the gamma-ray luminosity functions of the same sources and see if they can produce the required neutrino flux. Gamma-ray production is a natural consequence if one is using the pion decay model for neutrino production. In this way, one could more easily constrain the neutrino production with the gamma-ray production. This is however outside the scope of this paper and will be left for future work.

8 Conclusion

References

- Aab, A. et al. (Sept. 2020). “Features of the Energy Spectrum of Cosmic Rays above 2.5 Using the Pierre Auger Observatory”. In: *Phys. Rev. Lett.* 125 (12), p. 121106. DOI: 10.1103/PhysRevLett.125.121106. URL: <https://link.aps.org/doi/10.1103/PhysRevLett.125.121106>.
- Abbasi, R. et al. (Mar. 2022). “Improved Characterization of the Astrophysical Muon-neutrino Flux with 9.5 Years of IceCube Data”. In: *The Astrophysical Journal* 928.1, p. 50. DOI: 10.3847/1538-4357/ac4d29. URL: <https://dx.doi.org/10.3847/1538-4357/ac4d29>.
- Abdul Halim, A. et al. (2023). “Constraining the sources of ultra-high-energy cosmic rays across and above the ankle with the spectrum and composition data measured at the Pierre Auger Observatory”. In: *Journal of Cosmology and Astroparticle Physics* 2023.05, p. 024. ISSN: 1475-7516. DOI: 10.1088/1475-7516/2023/05/024. URL: <http://dx.doi.org/10.1088/1475-7516/2023/05/024>.
- Abramowicz, Marek A. and Dr. Odele Straub (2023). *Accretion Discs*. 3.12.2023. URL: http://www.scholarpedia.org/article/Accretion_discs.
- Ajello, M. et al. (2009). “THE EVOLUTION OF SWIFT/BAT BLAZARS AND THE ORIGIN OF THE MeV BACKGROUND”. In: *The Astrophysical Journal* 699.1, p. 603. DOI: 10.1088/0004-637X/699/1/603. URL: <https://dx.doi.org/10.1088/0004-637X/699/1/603>.
- Alves Batista, Rafael et al. (June 2019). “Open Questions in Cosmic-Ray Research at Ultrahigh Energies”. In: *Frontiers in Astronomy and Space Sciences* 6. ISSN: 2296-987X. DOI: 10.3389/fspas.2019.00023. URL: <http://dx.doi.org/10.3389/fspas.2019.00023>.
- Andeen, Karen and Matthias Plum (Jan. 2019). “Latest Cosmic Ray Results from IceTop and IceCube”. In: *EPJ Web of Conferences* 210, p. 03005. DOI: 10.1051/epjconf/201921003005.
- Andrews, Henrik (2023). *Master project*. URL: <https://github.com/henan99/Master-Project>.
- Bian, Wei-Hao and Yong-Heng Zhao (June 2003). “Accretion Rates and the Accretion Efficiency in AGNs”. In: *Publications of the Astronomical Society of Japan* 55.3, pp. 599–603. ISSN: 0004-6264. DOI: 10.1093/pasj/55.3.599. eprint: <https://academic.oup.com/pasj/article-pdf/55/3/599/17447902/pasj55-0599.pdf>. URL: <https://doi.org/10.1093/pasj/55.3.599>.
- Blandford, R. D. and R. L. Znajek (July 1977). “Electromagnetic extraction of energy from Kerr black holes”. In: *Monthly Notices of the Royal Astronomical Society* 179.3, pp. 433–456. ISSN: 0035-8711. DOI: 10.1093/mnras/179.3.433. eprint: <https://academic.oup.com/mnras/article-pdf/179/3/433/9333653/mnras179-0433.pdf>. URL: <https://doi.org/10.1093/mnras/179.3.433>.
- BUeda, Yoshihiro et al. (Apr. 2014). “TOWARD THE STANDARD POPULATION SYNTHESIS MODEL OF THE X-RAY BACKGROUND: EVOLUTION OF X-RAY LUMINOSITY AND ABSORPTION FUNCTIONS OF ACTIVE GALACTIC NUCLEI INCLUDING COMPTON-THICK POPULATIONS”. In: *The Astrophysical Journal* 786.2, p. 104. DOI: 10.1088/0004-637X/786/2/104. URL: <https://dx.doi.org/10.1088/0004-637X/786/2/104>.
- Collaboration, The Pierre Auger et al. (2017). *The Pierre Auger Observatory: Contributions to the 35th International Cosmic Ray Conference (ICRC 2017)*. arXiv: 1708.06592 [astro-ph.HE].
- Dermer, Charlees D. and Govind Menon (2009). *High Energy Radiation from Black Holes: Gamma Rays, Cosmic Rays, and Neutrinos*. Princeton University Press.
- Garofalo, David et al. (Jan. 2019). “The redshift distribution of BL Lacs and FSRQs”. In: *Research in Astronomy and Astrophysics* 19.1, p. 013. ISSN: 1674-4527. DOI: 10.1088/1674-4527/19/1/13. URL: <http://dx.doi.org/10.1088/1674-4527/19/1/13>.
- Hillas, A. M. (1984). “The Origin of Ultra-High-Energy Cosmic Rays”. In: *Annual Review of Astronomy and Astrophysics* 22.1, pp. 425–444. DOI: 10.1146/annurev.aa.22.090184.002233. URL: <https://doi.org/10.1146/annurev.aa.22.090184.002233>.
- Hogg, David W. (2000). *Distance measures in cosmology*. arXiv: astro-ph/9905116 [astro-ph].
- Kotera, Kumiko and Angela V. Olinto (2011). “The Astrophysics of Ultrahigh-Energy Cosmic Rays”. In: *Annual Review of Astronomy and Astrophysics* 49.1, pp. 119–153. DOI: 10.1146/annurev-astro-081710-102620. eprint: <https://doi.org/10.1146/annurev-astro-081710-102620>. URL: <https://doi.org/10.1146/annurev-astro-081710-102620>.

- Kurahashi, Naoko, Kohta Murase, and Marcos Santander (Sept. 2022). “High-Energy Extragalactic Neutrino Astrophysics”. In: *Annual Review of Nuclear and Particle Science* 72.1, pp. 365–387. ISSN: 1545-4134. DOI: 10.1146/annurev-nucl-011122-061547. URL: <http://dx.doi.org/10.1146/annurev-nucl-011122-061547>.
- Laha, Suvendu et al. (Jan. 2021). “Ionized outflows from active galactic nuclei as the essential elements of feedback”. In: *Nature Astronomy* 5.1, pp. 13–24. ISSN: 2397-3366. DOI: 10.1038/s41550-020-01255-2. URL: <https://doi.org/10.1038/s41550-020-01255-2>.
- Madau, Piero and Mark Dickinson (Aug. 2014). “Cosmic Star-Formation History”. In: *Annual Review of Astronomy and Astrophysics* 52.1, pp. 415–486. ISSN: 1545-4282. DOI: 10.1146/annurev-astro-081811-125615. URL: <http://dx.doi.org/10.1146/annurev-astro-081811-125615>.
- Mason, Rachel E (2015). “Dust in the torus of the AGN unified model”. In: *Planetary and Space Science* 116. Cosmic Dust VII, pp. 97–101. ISSN: 0032-0633. DOI: <https://doi.org/10.1016/j.pss.2015.02.013>. URL: <https://www.sciencedirect.com/science/article/pii/S0032063315000483>.
- Narumoto, Takuro and Tomonori Totani (May 2006). “Gamma-Ray Luminosity Function of Blazars and the Cosmic Gamma-Ray Background: Evidence for the Luminosity-Dependent Density Evolution”. In: *The Astrophysical Journal* 643.1, pp. 81–91. ISSN: 1538-4357. DOI: 10.1086/502708. URL: <http://dx.doi.org/10.1086/502708>.
- Netzer, Hagai (2015). “Revisiting the Unified Model of Active Galactic Nuclei”. In: *Annual Review of Astronomy and Astrophysics* 53.1, pp. 365–408. DOI: 10.1146/annurev-astro-082214-122302. URL: <https://doi.org/10.1146/annurev-astro-082214-122302>.
- Palladino, Andrea et al. (Apr. 2020). “Can astrophysical neutrinos trace the origin of the detected ultra-high energy cosmic rays?” In: *Monthly Notices of the Royal Astronomical Society* 494.3, p. 4255–4265. ISSN: 1365-2966. DOI: 10.1093/mnras/staa1003. URL: <http://dx.doi.org/10.1093/mnras/staa1003>.
- Raimundo, S. I. et al. (Jan. 2012). “Can we measure the accretion efficiency of active galactic nuclei?” In: *Monthly Notices of the Royal Astronomical Society* 419.3, pp. 2529–2544. ISSN: 0035-8711. DOI: 10.1111/j.1365-2966.2011.19904.x. eprint: <https://academic.oup.com/mnras/article-pdf/419/3/2529/18717746/mnras0419-2529.pdf>. URL: <https://doi.org/10.1111/j.1365-2966.2011.19904.x>.
- Sanders, Nathan (2021). *Guide to Classification of Galaxies and AGNs*. 15.11.2023. URL: <https://astrobites.org/guides/galaxy-and-agn-types/>.
- Shields, Gregory A. (1999). “A Brief History of Active Galactic Nuclei”. In: *Publications of the Astronomical Society of the Pacific* 111.760, pp. 661–678. DOI: 10.1086/316378. URL: <https://doi.org/10.1086/316378>.
- Silverman, J. D. et al. (May 2008). “The Luminosity Function of X-Ray-selected Active Galactic Nuclei: Evolution of Supermassive Black Holes at High Redshift”. In: *The Astrophysical Journal* 679.1, p. 118. DOI: 10.1086/529572. URL: <https://dx.doi.org/10.1086/529572>.
- Stanev, Todor (June 2009). “Propagation of ultrahigh-energy cosmic rays”. In: *New Journal of Physics* 11.6, p. 065013. DOI: 10.1088/1367-2630/11/6/065013. URL: <https://dx.doi.org/10.1088/1367-2630/11/6/065013>.
- Ueda, Yoshihiro et al. (2003). “Cosmological Evolution of the Hard X-Ray Active Galactic Nucleus Luminosity Function and the Origin of the Hard X-Ray Background”. In: *The Astrophysical Journal* 598.2, p. 886. DOI: 10.1086/378940. URL: <https://dx.doi.org/10.1086/378940>.
- Walg, S. et al. (June 2013). “Relativistic AGN jets I. The delicate interplay between jet structure, cocoon morphology and jet-head propagation”. In: *Monthly Notices of the Royal Astronomical Society* 433.2, pp. 1453–1478. ISSN: 0035-8711. DOI: 10.1093/mnras/stt823. eprint: <https://academic.oup.com/mnras/article-pdf/433/2/1453/4923906/stt823.pdf>. URL: <https://doi.org/10.1093/mnras/stt823>.